Surface tension of supercooled water nanodroplets from computer simulations

Shahrazad M. A. Malek (ID), Peter H. Poole (ID), and Ivan Saika-Voivod (ID)

View Online   Export Citation   CrossMark

Surface tension of supercooled water nanodroplets from computer simulations

View Online   Export Citation   CrossMark

Shahrazad M. A. Malek,[1] [ID] Peter H. Poole,[2] [ID] and Ivan Saika-Voivod[1,a] [ID]

AFFILIATIONS

[1] Department of Physics and Physical Oceanography, Memorial University of Newfoundland, St. John's,
Newfoundland A1B 3X7, Canada

[2] Department of Physics, St. Francis Xavier University, Antigonish, Nova Scotia B2G 2W5, Canada

Note: This paper is part of a JCP Special Topic on Chemical Physics of Supercooled Water.

[a] saika@mun.ca

ABSTRACT

We estimate the liquid-vapor surface tension from simulations of TIP4P/2005 water nanodroplets of size $N = 100$ to 2880 molecules over a temperature T range of 180 K–300 K. We compute the planar surface tension γ_p, the curvature-dependent surface tension γ_s, and the Tolman length δ, via two approaches, one based on the pressure tensor (the "mechanical route") and the other on the Laplace pressure (the "thermodynamic route"). We find that these two routes give different results for γ_p, γ_s, and δ although in all cases, we find that $\delta \geq 0$ and is independent of T. Nonetheless, the T dependence of γ_p is consistent between the two routes and with that of Vega and de Miguel [J. Chem. Phys. **126**, 154707 (2007)] down to the crossing of the Widom line at 230 K for ambient pressure. Below 230 K, γ_p rises more rapidly on cooling than predicted from behavior for $T \geq 300$ K. We show that the increase in γ_p at low T is correlated with the emergence of a well-structured random tetrahedral network in our nanodroplet cores and thus that the surface tension can be used as a probe to detect behavior associated with the proposed liquid-liquid phase transition in supercooled water.

Published under license by AIP Publishing. https://doi.org/10.1063/1.5096990

I. INTRODUCTION

Microscopic and nanoscopic water droplets are of interest in many important research areas, such as the Earth's climate,[1,2] biological applications,[3] interstellar space,[4] and numerous other systems.[5] In all of these areas, the surface tension of the liquid-vapor interface of the water droplet is a central physical property for understanding and predicting droplet behavior. For example, the surface tension is crucial for estimating the nucleation rate of liquid from the vapor using classical nucleation theory.[6,7]

The surface tension is also the origin of the pressure difference that arises between the interior and exterior of a liquid droplet, as quantified by the Young-Laplace equation,[8,9]

$$\Delta P = \frac{2\gamma_s}{R_s}. \tag{1}$$

Here, $\Delta P = P_l - P_v$, where P_l and P_v are the respective pressures of the liquid interior and vapor exterior, and γ_s is the surface tension of the curved interface. R_s is the radius of the so-called "surface of tension."[10] For macroscopic droplets, the width of the molecular interface is negligible compared to the droplet dimensions, and R_s is simply the radius of the droplet. However, for nanoscale droplets, the interfacial width is significant compared to the size of the droplet itself, and various definitions for the radius of the droplet are possible.

It has long been understood that the surface tension of a curved interface deviates from that of a planar interface. For a curved surface, such as that of a droplet, the Tolman length δ quantifies how γ_s deviates from the planar surface tension γ_p as a function of R_s, via the expression[11]

$$\gamma_s = \frac{\gamma_p}{(1 + 2\delta/R_s)}. \tag{2}$$

The magnitude of δ is generally found to be 10%–20% of the molecular diameter.

However, the sign of δ is a subject of continuing debate.[12] While modeling on the basis of classical density functional theory has predicted negative values of δ for liquid Lennard-Jones (LJ)

droplets,[13,14] simulations of droplets have estimated both negative and positive values of δ. For example, Yan et al.[15] performed molecular dynamics (MD) simulations of liquid argon nanodroplets with sizes ranging from 800 to 2000 atoms at 78 K, as modeled using the LJ potential. They evaluated the pressure tensor, and using the Young-Laplace equation, they concluded that δ is positive for LJ nanodroplets. However, van Giessen and Blokhuis[12] estimated a negative value of δ for LJ nanodroplets.

A similar disagreement regarding the magnitude and sign of δ appears in water simulations. Leong and Wang[16] performed MD simulations using the BLYPSP-4F water potential[17] on nanoscale droplets with radii varying between 2 and 8 nm at temperature $T = 298$ K. Using an empirical correlation between the pressure and density, they estimated $\delta = -0.048$ nm. A similar value for δ was obtained by measuring the free energy of droplet mitosis in a study by Joswiak et al.[18] for the mW model of water.[19] On the other hand, Lau et al.[20] used a test-area method and obtained a positive value of δ for the TIP4P/2005 model of water.[21] Simulation studies of cavitation for TIP4P/2005 find relatively large positive values of δ for vapor bubbles with magnitudes in the range of 0.12–0.195 nm.[22,23] This result implies that for a TIP4P/2005 water droplet of the same size, δ should be of similar magnitude but negative. It is evident from this recent work that disagreement exists on both the magnitude and sign of δ, even when the same water model is used.

The variation of the surface tension with T for deeply supercooled water has also been investigated, in particular as a way to test for evidence of a possible liquid-liquid phase transition (LLPT) in supercooled water.[24] Theoretical studies have shown that if a LLPT occurs, then at low T, the surface tension should increase faster with decreasing T than is expected otherwise.[25–27] Some computer simulations studies are consistent with this behavior,[28,29] while others are not.[30,31] Recent careful experiments by Hruby and coworkers do not find evidence for a change in the T dependence of the surface tension for T as low as $-26\,°C$.[32–34] However, it is possible that the anomalous increase in the surface tension will only be observed for T below the Widom line that is associated with the LLPT, a range of T that has only recently begun to be probed in experiments.[35]

The sign of δ determines whether γ_s decreases or increases with R_s. For a positive δ, γ_s decreases as R_s decreases. Moreover, δ relates the equimolar radius R_e and R_s[11]

$$\delta = R_e - R_s, \tag{3}$$

where R_e is the radius of a sphere that has a uniform density equal to that of the interior part of the droplet and that has the same number of molecules as the droplet. Since determining R_e is more straightforward than determining R_s, we can rewrite Eqs. (1) and (2) in terms of R_e

$$\Delta P = \frac{2\gamma_p}{R_e}\left(\frac{1}{1 + \delta/R_e}\right), \tag{4}$$

or in the form

$$\frac{2}{\Delta P R_e} = \frac{1}{\gamma_p}(1 + \delta/R_e), \tag{5}$$

and

$$\gamma_s = \gamma_p \frac{R_e - \delta}{R_e + \delta}. \tag{6}$$

The above equations provide the basis for a procedure to find γ_p, γ_s, and δ, which following past practice we refer to here as the "thermodynamic route."[36] As we will see below, computer simulations of water nanodroplets allow us to directly estimate ΔP and R_e. If we obtain ΔP and R_e for a range of droplet sizes at fixed T, we can use Eq. (5) to estimate γ_p and δ by curve fitting. From δ, an estimate of R_s is obtained from Eq. (3), and so an estimate of γ_s can be computed using Eq. (1).

Aside from the Laplace equation, Rowlinson and Widom proposed a model to derive γ_s from the tangential and normal components of the pressure tensor as functions of the radial distance r from the center of mass of a droplet, $P_T(r)$ and $P_N(r)$.[10] The model assumes two homogeneous fluid phases, with homogeneous pressures P^α and P^β far from the interface, and an inhomogeneous interface between them. Under the model assumption that the surface tension acts at a single value of $r = R_s$, the mechanical requirements for static equilibrium, i.e., force and torque balance, yield

$$\gamma_s = \int_0^\infty \left(\frac{r}{R_s}\right)\left[P^{\alpha,\beta}(r; R_s) - P_T(r)\right]dr, \tag{7}$$

$$= \int_0^\infty \left(\frac{r}{R_s}\right)^2\left[P^{\alpha,\beta}(r; R_s) - P_T(r)\right]dr, \tag{8}$$

where $P^{\alpha,\beta}(r; R_s)$ is P^α for $r < R_s$ and P^β for $r > R_s$. These equations in turn give an expression for R_s

$$R_s = \frac{\int_0^\infty r^2\left[P^{\alpha,\beta}(r; R_s) - P_T(r)\right]dr}{\int_0^\infty r\left[P^{\alpha,\beta}(r; R_s) - P_T(r)\right]dr}. \tag{9}$$

With the assumption that the two phases are homogeneous, we can assume that $P^\alpha = P_l$ and $P^\beta = P_v$. Since $P^{\alpha,\beta}(r; R_s)$ depends on R_s, Eq. (9) must be evaluated numerically.

From the condition of mechanical stability, $\nabla \cdot \mathbf{P} = 0$, it can be shown that

$$\int_0^\infty r^2\left[P^{\alpha,\beta}(r; R_s) - P_N(r)\right]dr = 0, \tag{10}$$

and hence, γ_s can be obtained using the $P_N(r)$ component of the pressure in Eqs. (7) and (8), yielding

$$\gamma_s = \int_0^\infty \left(\frac{r}{R_s}\right)^2\left[P_N(r) - P_T(r)\right]dr, \tag{11}$$

and[10]

$$R_s = \frac{\int_0^\infty r^2[P_N(r) - P_T(r)]dr}{\int_0^\infty r[P_N(r) - P_T(r)]dr}. \tag{12}$$

We can also find γ_s while avoiding the need for R_s by combining Eqs. (1) and (11)

$$\gamma_s^3 = \frac{(P_l - P_v)^2}{4}\int_0^\infty r^2[P_N(r) - P_T(r)]dr. \tag{13}$$

Equations (7)–(13) provide an alternative pathway, referred to as the "mechanical route,"[36] to compute γ_s and R_s, as well as γ_p and δ. First, $P_N(r)$ and $P_T(r)$ are calculated from simulations of nanodroplets, with Eqs. (7)–(13) yielding values for γ_s and R_s. Estimates for γ_p and δ are then obtained through Eqs. (2) and (3).

In this study, we use the TIP4P/2005 model to simulate water nanodroplets over a wide range of temperatures and sizes and determine γ_s, γ_p, and δ using both the thermodynamic and mechanical routes. In Sec. II, we provide details of our simulations. In Secs. III–V, we show that the thermodynamic and mechanical routes give different results for the surface tension and Tolman length for water. Despite these differences, we find that all methods demonstrate that γ_p increases more rapidly upon cooling through the Widom line temperature for TIP4P/2005. In Sec. VI, we show that the rapid increase in γ_p at low T is consistent with a crossover within the core of our nanodroplets from the high density liquid (HDL) phase to the low density liquid (LDL) phase of the LLPT. We present a discussion and our conclusions in Sec. VII.

II. SIMULATIONS

We recently studied the thermodynamic and structural properties of simulated water nanodroplets ranging in size from $N = 100$ to 2880 molecules, over a T range of 180–300 K,[37] with molecules interacting through the TIP4P/2005 model.[21] The same data set is used in the present study. We summarize the simulation details below for the reader's convenience.

We carry out the simulations in the canonical ensemble—constant N, volume V, and temperature T. The droplets are located in a periodic cubic box of side length L that increases with N and ranges from 10 to 20 nm. We ensure the box is large enough to avoid any direct interaction between the water droplet and its periodic images and small enough to ensure that at most only a few molecules are in the vapor phase. We use a potential cutoff of $L/2$, ensuring that all molecules in the droplet interact without truncation of the potential. We use Gromacs v4.6.1[38] to carry out our molecular dynamics (MD) simulations. We hold the temperature constant using the Nosé-Hoover thermostat with time constant 0.1 ps. The equations of motion are integrated with the leap-frog algorithm with a time step of 2 fs.

The data set is generated from two kinds of MD runs: conventional "single long runs" (SLR) and using a "swarm relaxation" method (SWRM).[39] For droplet sizes $N = 100, 200, 360, 776, 1100, 1440,$ and 2880, we use SLRs. For $N = 1440$ and 2880, we start our simulations by placing N molecules randomly within the simulation box and run long enough for the molecules to condense into a single droplet. We harvest an equilibrated $N = 1440$ configuration and progressively remove molecules from the droplet surface to obtain starting configurations for the other droplet sizes. The slowest relaxation times are approximately 12 ns, and our longest postequilibration simulations last 2.8 μs.

For droplet sizes $N = 205, 301, 405, 512, 614,$ and 729, we use SWRM. To generate initial configurations for each of these droplet sizes, we first remove molecules from the surface of an equilibrated $N = 2880$ configuration to obtain the desired size. We first conduct SLRs for each size at $T = 200$ K for not less than 350 ns. We then take the last configuration of each run and randomize the velocities using the Maxwell-Boltzmann distribution at $T = 220$ K to generate M different configurations, which are used to initiate our swarm relaxation runs. We determine the relaxation time τ_s for a swarm ensemble from the potential energy autocorrelation function of the system. See Ref. 39 for details. The final equilibrated M configurations of the ensemble are then used to initiate an ensemble of runs

at $T = 200$ K. Similarly, we take the final equilibrated M configurations of the ensemble at $T = 200$ K to start a swarm ensemble at $T = 180$ K.

Additionally, we carry out simulations for bulk liquid TIP4P/2005 with T varying from 300 to 180 K. We simulate 360 molecules with density varying approximately between 0.96 and 1.12 g/cm^3 using the protocols described in Ref. 40.

The mechanical route to finding the surface tension of a droplet requires the determination of both $P_T(r)$ and $P_N(r)$. We compute kinetic and configurational contributions to the pressure inside our droplets; see Ref. 41 for details on applying to TIP4P/2005 a coarse-grained method[42] based on the Irving-Kirkwood[43] choice of contour in defining the microscopic pressure. Figure 1 shows all contributions to the pressure for two example cases. We define R_L such that the configurational contributions to the normal and tangential pressures, $P_{c,N}$ and $P_{c,T}$, respectively, are equal to each other within error for $r < R_L$ (dashed line in Fig. 1), noting that they differ near the surface. To define the pressure in the interior of the droplets P_L, we average the total (isotropic) pressure $P_{tot}(r) = P_{c,N}(r)/3 + 2P_{c,T}(r)/3 + \rho_\circ(r)k_B T$ over the spherical volume of radius R_L, where $\rho_\circ(r)$ is the local number density.

All error bars reported in this work indicate one standard deviation in the mean.
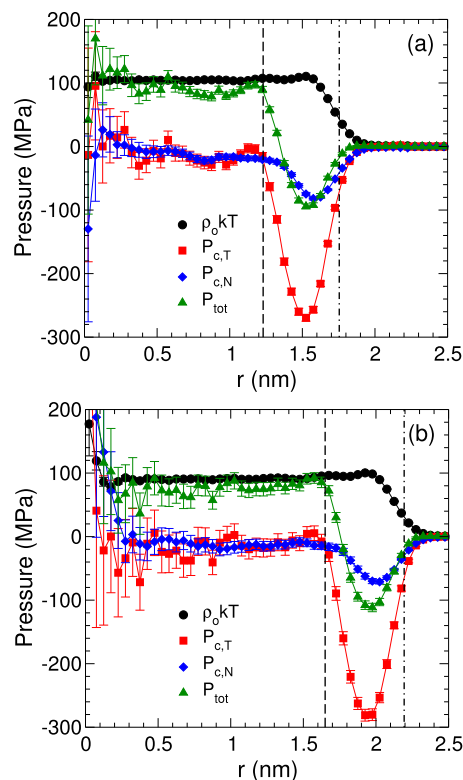

FIG. 1. Contributions to the pressure inside water nanodroplets as a function of r, for (a) $N = 776$ and $T = 220$ K and (b) $N = 1440$ and $T = 200$ K. Vertical lines identify $r = R_L$ (dashed line) and $r = R_e$ (dotted-dashed line).
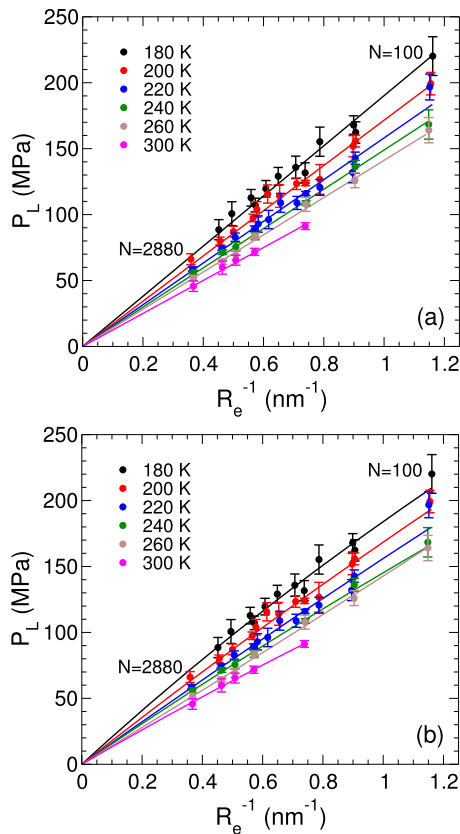
FIG. 2. Isotherms of P_L as a function of R_e^{-1}. Along each isotherm, N decreases with R_e^{-1}. (a) The straight lines are one-parameter fits to Eq. (4) with the assumption that $\delta = 0$. (b) The curves are two-parameter fits to Eq. (4).
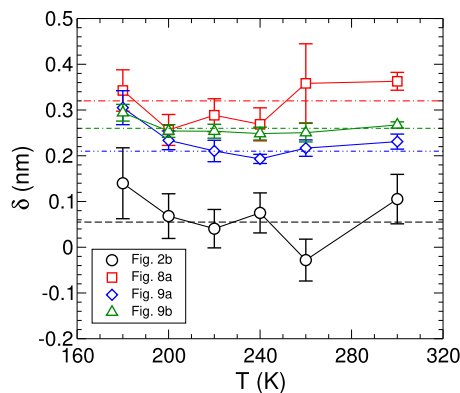

FIG. 3. Tolman length δ as a function of T obtained by different means: fits of $P_L(R_e)$ to Eq. (4) shown in Fig. 2(b) (black circles) with an average value of 0.055 ± 0.021 nm (dashed line); fits of $\gamma_s(R_s)$ to Eq. (2) shown in Fig. 8(a) (red squares) with an average value of 0.32 ± 0.02 nm (dotted-dashed line); fits of $\gamma_s(R_s)$ to Eq. (2) shown in Fig. 9(a) (blue diamonds) with an average value of 0.21 ± 0.01 nm (dotted-dotted-dashed line); and fits of $\gamma_s(R_e)$ to Eq. (6) shown in Fig. 9(b) (green triangles) with an average value of 0.26 ± 0.005 nm (dotted-dashed-dashed). The top three curves are from the mechanical route, while the bottom curve (black circles) is from the thermodynamic route.
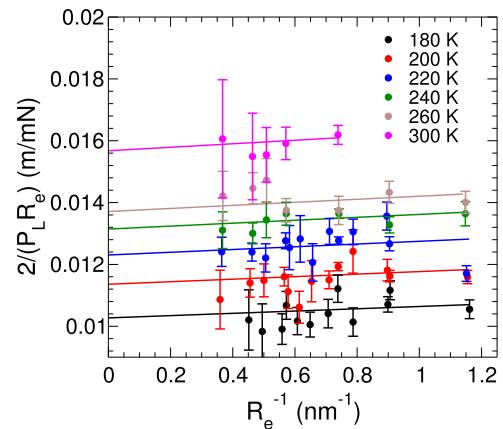

FIG. 4. Isotherms of $2/(P_L R_e)$ as a function of R_e^{-1}. Along each isotherm, N decreases with R_e^{-1}. The straight lines are fits to Eq. (5), where $\delta = 0.056$ nm is a global fit parameter.
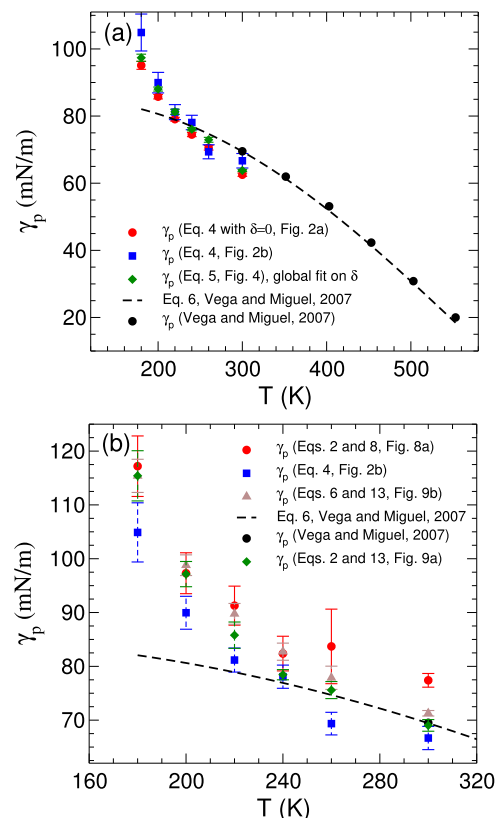
FIG. 5. The variation of planar surface tension γ_p with T. (a) γ_p via the thermodynamic route obtained from the fits in Fig. 2(a) (red circles), Fig. 2(b) (blue squares), and Fig. 4 (green diamonds). (b) γ_p via the mechanical route obtained from the fits in Fig. 8(a) (red circles), Fig. 9(a) (green diamonds), and Fig. 9(b) (brown triangles). Thermodynamic route results from Fig. 2(b) (blue squares) are added for comparison.

III. THERMODYNAMIC ROUTE

In the thermodynamic route, we use the Young-Laplace equation in the form of Eq. (4) to determine γ_p and δ. We equate P_L with ΔP since the vapor pressure is negligible and plot isotherms of P_L as a function of R_e^{-1} in Fig. 2. The isotherms show that there is a significant pressure that naturally builds up in the interior of the droplets, and it can reach more than 200 MPa for $R_e^{-1} \simeq 1.2$ nm^{-1} ($R_e \simeq 0.83$ nm).

In Fig. 2, we study the curvature correction to P_L as a function of R_e. Assuming $\delta = 0$, the fits in Fig. 2(a) using Eq. (4) (fitting only for γ_p) show that there is no obvious curvature correction to the Young-Laplace equation. To see how small δ is in our range of droplet sizes, we fit P_L as a function of R_e^{-1} at each T with Eq. (4) (fitting for both γ_p and δ), as shown in Fig. 2(b). We report the value of δ as a function of T in Fig. 3 and can discern no clear dependence of δ on T. The average small (positive) value of the Tolman length $\bar{\delta} = 0.055$ nm explains the absence of strong curvature in the isotherms of Fig. 2. As an alternative way of obtaining γ_p and δ, we plot isotherms of $2/(P_L R_e)$ as functions of R_e^{-1} in Fig. 4. Since δ does not have an apparent dependence on T, we fit the isotherms in Fig. 4 to Eq. (5) assuming a single common value of the fitting parameter δ for all T. As shown in Fig. 4, this global fit reasonably describes all the isotherms and gives a value of $\delta = 0.056$ nm that is similar to $\bar{\delta}$.
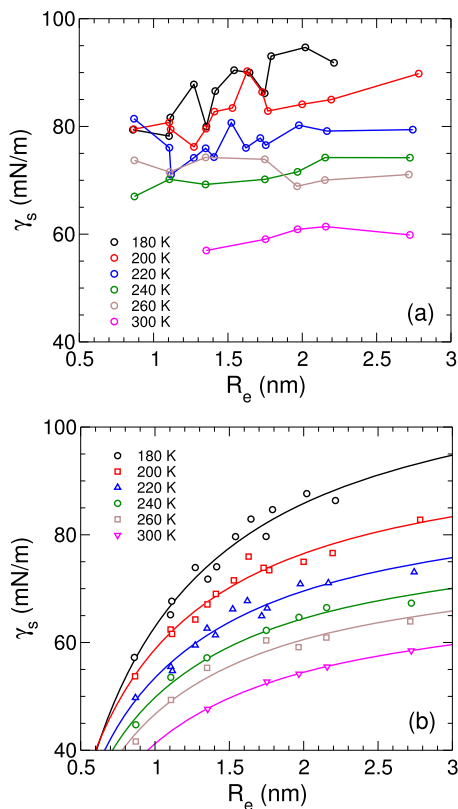

FIG. 7. γ_s as a function of R_e at $T = 300$ K from Eq. (8) (red squares); Eq. (13) (blue diamonds); using $\gamma_s = P_L (R_e - \delta)/2$ with $\delta = 0.105$ nm obtained from Fig. 2(b) (green triangles); and from Lau *et al.*[20] at $T = 293$ K (black circles).

The intercepts in Fig. 4 yield $1/\gamma_p$ for each T. As shown in Fig. 5(a), the values of γ_p obtained in this way increase as T decreases.

In Fig. 5(a), we compare estimates for γ_p assuming $\delta = 0$ [obtained from the fits in Fig. 2(a)] and $\delta \neq 0$ [obtained from the fits

FIG. 6. Isotherms of γ_s as a function of R_e. (a) γ_s obtained from the thermodynamic route, $\gamma_s = P_L (R_e - \delta)/2$. (b) γ_s obtained from the mechanical route through Eq. (13). Curves are fits to Eq. (6).
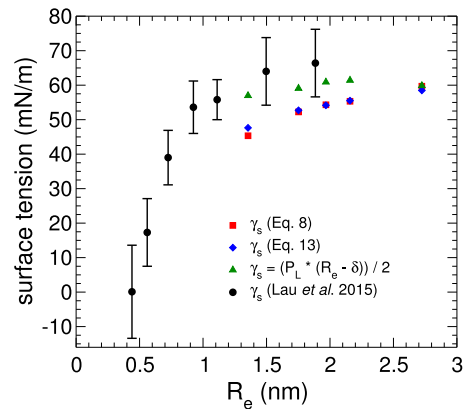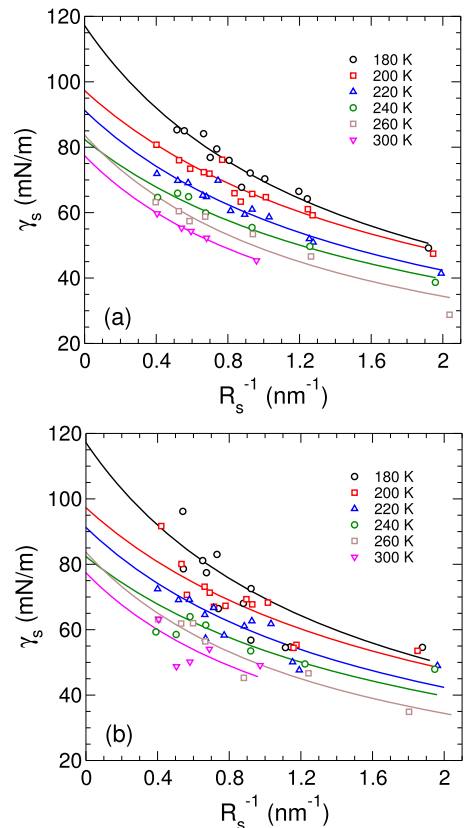

FIG. 8. γ_s as a function of R_s^{-1}. (a) γ_s obtained from Eq. (8) (symbols), where curves are fits to Eq. (2). (b) γ_s obtained from Eq. (11) (symbols), where curves are replotted from panel (a). Curve intercepts estimate γ_p.

in Fig. 2(b)]. At $T = 180$ K, the discrepancy in γ_p between assuming $\delta = 0$ and $\delta \neq 0$ appears to be outside of error, with the curvature-corrected result yielding a value of γ_p approximately 10% higher [blue squares vs red circles in Fig. 5(a)]. For $T \geq 220$ K, our estimates of γ_p are also consistent with the extrapolation down to low T of γ_p obtained using the test-area method, taken from Eq. (6) in the work of Vega and de Miguel.[44]

To obtain γ_s from the thermodynamics route, we combine Eqs. (1) and (3) to obtain $\gamma_s = P_L (R_e - \delta)/2$ and use the values of δ for each T obtained from fits shown in Fig. 2(b). The resulting values of γ_s are shown in Figs. 6(a) and 7.

IV. MECHANICAL ROUTE

As discussed in Sec. I, γ_p and δ can also be obtained using the mechanical route. To find γ_p and δ, we first evaluate γ_s using Eq. (8), where we set $P^\alpha = P_L$ and $P^\beta = 0$ since the vapor pressure in our simulations is negligible. In Fig. 8(a), we show isotherms of γ_s as a function of R_s^{-1}, where R_s is obtained from Eq. (9). We see that γ_s decreases with increasing R_s^{-1} along isotherms, indicating that δ is positive. Fitting these isotherms with Eq. (2) yields curves from which γ_p is estimated from the intercept at $R_s^{-1} = 0$. Our results for γ_p obtained in this way are shown in Fig. 5(b).

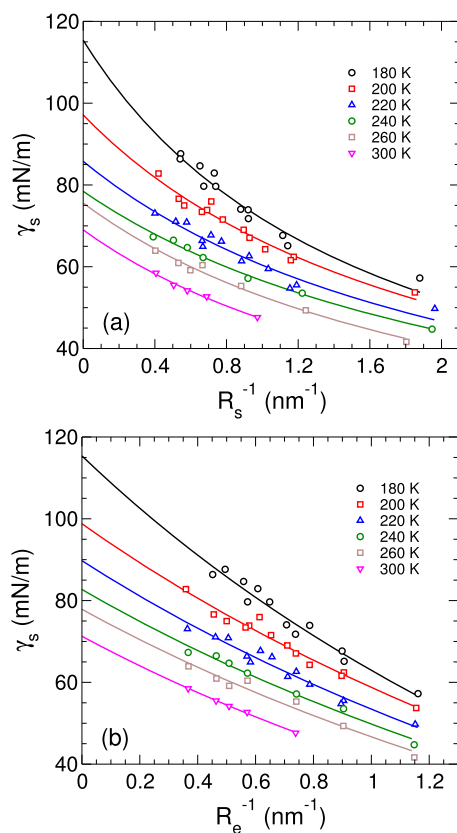**FIG. 9**. γ_s from Eq. (13) as a function of (a) R_s^{-1}, with fits to Eq. (2) (solid lines). (b) R_e^{-1}, with fits to Eq. (6) (solid lines). Curve intercepts estimate γ_p.

Another way of evaluating γ_s is through Eq. (11). Isotherms of γ_s from Eq. (11) as a function of R_s^{-1}, where R_s^{-1} is estimated using Eq. (12), are shown in Fig. 8(b). Although the trend seems to indicate that γ_s decreases with R_s^{-1} using Eqs. (11) and (12), the noise resulting from subtracting $P_N(r)$ and $P_T(r)$ prevents useful fitting of γ_s. The solid curves shown in Fig. 8(b) are simply the fits taken from Fig. 8(a) and show a general consistency between using Eqs. (8) and (9) and using Eqs. (11) and (12), with the former set suffering from less statistical scatter.

Unlike both Eqs. (8) and (11), which require the determination of R_s to evaluate γ_s, Eq. (13) does not involve calculating R_s. We plot γ_s obtained from Eq. (13) as a function of R_s^{-1} in Fig. 9(a). We choose R_s from Eq. (12) because γ_s in Eq. (13) is derived from Eq. (11). The absence of R_s in Eq. (13) seems to suppress the noise from $P_N(r)$. We fit the isotherms in Fig. 9(a) to Eq. (2), and we obtain values of γ_p and δ similar to those obtained from the isotherms in Fig. 8(a), as shown in Figs. 5(b) and 3.

To avoid any difficulty inherent in calculating R_s, another way of representing γ_s is as a function of R_e^{-1}, as shown in Fig. 9(b). Regardless of which variant of the mechanical route is taken, we observe that γ_s decreases as R_e and R_s decrease, δ is positive with little evidence for a dependence on T, and γ_p increases as T decreases. The values of δ obtained from each variant of the mechanical route are shown for each T in Fig. 3.

V. COMPARISON OF THERMODYNAMIC AND MECHANICAL ROUTES

Figure 5(b) shows that the mechanical route yields values of γ_p approximately 10% larger than does the thermodynamic route although the trends with T are similar. The mechanical route values for γ_p are also generally higher than those from Vega and de Miguel.[44] However, the best agreement with Ref. 44 between $T = 240$ K and 300 K comes from using Eq. (13) for calculating γ_s, Eq. (12) for calculating R_s, and fitting the resulting isotherms [shown in Fig. 9(a)] with Eq. (2) to obtain γ_p and δ.

For all variants of both routes, γ_p shows a striking departure from the extrapolated low T behavior presented in Ref. 44. The sharper than expected increase in γ_p with decreasing T occurs between 220 and 240 K and is therefore consistent with crossing the Widom line at 230 K for bulk TIP4P/2005 at ambient pressure.[45] In order for bulk properties of the liquid to influence γ_p as obtained from nanodroplets, it is reasonable to expect that nanodroplet interiors are structurally similar to the bulk, an expectation for which we provide evidence in Sec. VI.

For an independent comparison of γ_s, we show in Fig. 7 our results for γ_s as a function of R_e as obtained from both the thermodynamic and mechanical routes at $T = 300$ K along with the values from Lau et al.[20] obtained using the test-area method at $T = 293$ K. We see that our results for γ_s from the thermodynamic route are consistent with Lau et al. However, the mechanical route gives significantly smaller values of γ_s. Smaller values of γ_s and R_s and larger values of δ for the mechanical route are also observed in nanodroplets interacting through the Lennard-Jones potential studied by Thompson et al.[36]

While Fig. 7 shows consistency in the value of γ_s and its R_e dependence between our thermodynamic route and the test-area method employed by Lau et al.,[20] other studies have found that

$\gamma_s \approx \gamma_p$ for droplets as small as approximately 40 molecules ($R_e \approx 0.6$ nm). These studies employed techniques including excision of spherical portions from a bulk liquid,[46] a volume perturbation method allowing for a thermodynamic determination of the pressure tensor components,[47] and a mitosis method by Joswiak *et al.*[18] Interestingly, Lau *et al.* also carried out a mitosis method in a different study[48] (also finding that γ_s depends more weakly on R_e) and offered some discussion on the disparity between the mitosis and test-area methods. All these other studies point to the validity of approximating γ_s with γ_p in estimating the Laplace pressure for very small nanodroplets.

To compare the difference in γ_s as obtained from the mechanical and thermodynamic routes, we plot in Fig. 6 isotherms of γ_s as a function of R_e. Figure 6(b) shows a significant change in γ_s obtained from Eq. (13) as droplet size varies. For a change in the nanodroplet radius from 1 to 3 nm, there is a 50% increase in γ_s at $T = 180$ K and 44% at $T = 300$ K. However, if we compare this with γ_s estimated from the thermodynamic route shown in Fig. 6(a), we see that the isotherms are almost flat for $T \geq 220$ K, while there is only a 15% difference in γ_s across the droplet size range for $T \leq 200$ K. We also can see that γ_s from the thermodynamic route is systematically larger than the mechanical route, which is once again consistent with the result of Thompson *et al.*[36]

As shown by Sampayo *et al.*,[49] disparity between thermodynamic and mechanical routes arises when energy fluctuations (and not merely the average change in energy) become important in determining the free energy change when surface area is increased. While for planar interfaces, such fluctuations do not contribute significantly to the surface tension, the contribution for small droplets can be significant. Thermodynamic routes include these fluctuations, while mechanical routes would require the addition of hyper-virial terms to include the effects of fluctuations. Ignoring these fluctuations in the mechanical route (i.e., when using pressure tensor components only) can lead, for example, to a change in sign in the determination of δ for Lennard-Jones droplets. See also Ref. 50 for discussion.

VI. LOCAL STRUCTURE ORDERING

To quantify the structure of the interior of our water nanodroplets, we calculate the distance $d_5(r)$ between a molecule located at a distance r from the center of the droplet and its fifth-nearest-neighbor molecule (using distances between centers of mass). A large value of $d_5(r)$ indicates that molecules tend to be four-coordinated, i.e., the local tetrahedral network is well formed.[51]

In Fig. 10(a), we show $d_5(r)$ over a wide range of N and T. We observe that $d_5(r)$ for droplet size $N = 100$ is small and stays rather constant with T. The low value of d_5 indicates a collapse of the second neighbor shell around each molecule. This collapse is characteristic of the HDL form of water. The absence of any change in $d_5(r)$ with r as we approach the surface indicates a disturbance in the tetrahedral network in the whole droplet. The overlap of the curves at different T for $N = 100$ suggests that droplets at this small size remain HDL-like both in the interior and at the surface regardless of how deeply we supercool them.

As we increase the droplet size to $N = 360$, the profiles systematically shift to a higher value of d_5 in the interior as we cool to 180 K.
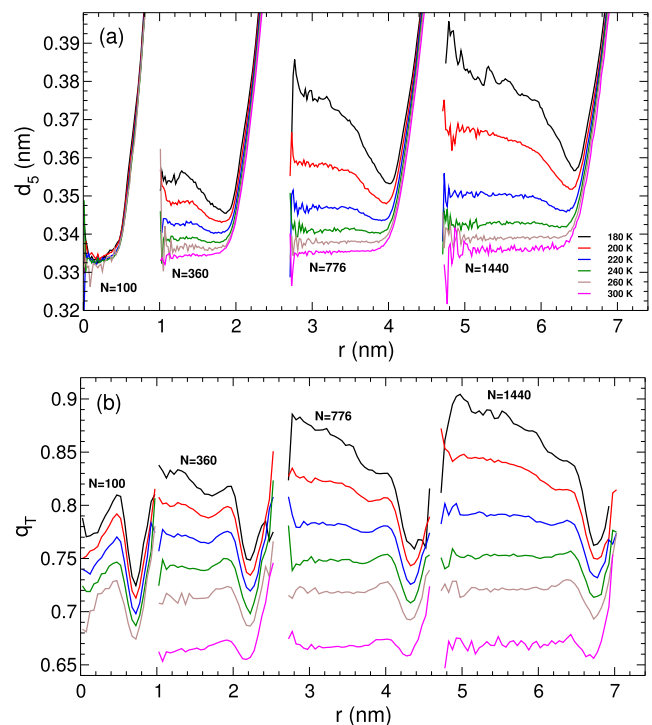

FIG. 10. (a) d_5 as a function of radius r for various N and T. The curves have been shifted horizontally by 1 nm for $N = 360$, by 2.7 nm for $N = 776$, and by 4.7 nm for $N = 1440$. (b) q_T as a function of radius r for various N and T. The curves have been shifted horizontally by 1 nm for $N = 360$, by 2.7 nm for $N = 776$, and by 4.7 nm for $N = 1440$.

This change is a signature of a crossover from HDL at high T to LDL at low T. However, for $T \leq 220$ K and $N = 360$ in Fig. 10(a), there is a decrease in d_5 going from interior to surface, which indicates a disturbance of the tetrahedral network and an increase in density at the surface. For larger droplets, such as $N = 776$, we see similar behavior as for $N = 360$, but the transformation spans a wider range of d_5. Moreover, for $N = 776$ at $T = 180$ K, we see a monotonic decrease in d_5 as we approach the surface. This may reflect the emergence of structural transformation within the droplet. The same scenario presents itself for $N = 1440$. At $T = 180$ K, as N increases from 100 to 1440, d_5 in the interior monotonically increases with N. This indicates that as N increases, a better LDL forms in the interior of the droplets.

To further probe the ordering inside the nanodroplets, we compute the local tetrahedral order parameter[52]

$$q_i = 1 - \frac{3}{8} \sum_{j=1}^{3} \sum_{k=j+1}^{4} \left[\cos \psi_{jik} + \frac{1}{3} \right]^2, \qquad (14)$$

where ψ_{jik} is the angle between an oxygen atom i and its nearest neighbor oxygen atoms j and k. Subsequently, we define $q_T(r)$ as the average value of q_i for all molecules within a spherical shell bounded by radii $r \pm \Delta r/2$, where $\Delta r = 0.05$ nm.

We show how $q_T(r)$ changes in Fig. 10(b). We see that q_T is low for $N = 100$ and it increases as we cool the droplet. Similar behavior

appears for $N = 360$, 776, and 1440. However, for $T = 200$ and 180 K, the increase in q_T upon increasing N becomes quite dramatic, supporting the suggestion that a better tetrahedral network forms as N increases. For $N = 1440$ at $T = 180$ K, the core reaches 90% of perfect tetrahedral order. The monotonic decrease in q_T with r for $N = 776$ and 1440 at $T = 180$ K is consistent with the decrease with r that we observe in d_5.

Our results for d_5 and q_T suggest the progressive formation of LDL-like structure in the interior of our droplets as T decreases. The structural results presented here are also consistent with the evolution of the density profiles of our droplets presented in Ref. 37. The transformation from HDL to LDL in the droplet interior can also explain the change in behavior in γ_p for $T < 240$ K shown in Fig. 5. Since LDL is a more structured liquid than HDL, with a better formed hydrogen bond network, we expect that the interface between LDL and the vapor phase will have a higher surface tension than for the interface between HDL and the vapor.

To illustrate the structurally bulklike character of our droplet interiors, we plot d_5 and q_T as functions of density in Fig. 11. To compute the density, we define the density within the core of our droplets as $\rho_c = m \langle \mathcal{N}/\mathcal{V} \rangle$, where $\mathcal{N}$ is the number of O atoms within a defined core radius $r_c = 0.5$ nm of the droplet center, $\mathcal{V}$ is the total

volume of the Voronoi cells for these atoms,[53] and m is the mass of a water molecule. Since in the smallest droplets, surface effects extend closer to the center of droplet, we use $r_c = 0.25$ nm for $N \leq 205$. Similarly, we define d_5 and q_T for droplet interiors by averaging the corresponding local quantities for particles within r_c of the droplet center (molecules for d_5 and O atoms for q_T). Figure 11 shows the agreement between d_5 and q_T as functions of density for bulk systems and droplets. This correspondence demonstrates that the core of the droplets for our range of N is bulklike. These structurally bulklike interiors are consistent with the possibility that our extrapolated values of γ_p, obtained from the behavior of nanoscale droplets, approximate those for bulk planar liquid-vapor interfaces and hence that the anomalous increase in γ_p we observe below 230 K reflects the bulk liquid anomalies associated with crossing the Widom line of the LLPT.

VII. DISCUSSION AND CONCLUSIONS

We estimate the surface tension of water nanodroplets using the TIP4P/2005 model over a wide range of N and T. We do so from an evaluation of the components of the pressure tensor inside the droplets[37] using the method described in Ref. 41. From the pressure tensor components, we determine the isotropic pressure P_L in the interior of the droplets. This allows us to calculate the surface tension with two approaches: using the Young-Laplace equation directly and using the variation of the pressure tensor components with distance from the droplet center. The direct route, which we call the thermodynamic route, requires P_L and R_e to estimate γ_s, γ_p, and δ as fit parameters, and the mechanical route evaluates γ_s and R_s from the pressure tensor components and yields γ_p and δ from fitting. It should be noted, however, that the analysis carried out by Gibbs (see Ref. 10) and reiterated by Tolman[11] implies that the interior pressure that should be used in Eq. (1) is that of the bulk fluid with the same chemical potential as the droplet interior. It would be interesting to quantify the differences in the calculated surface tension that arise from using this definition instead of the directly calculated pressure, particularly for smaller droplets where differences may be significant.

Isotherms of P_L plotted as a function of R_e^{-1} on the assumption that the surface of tension acts at R_e (i.e., $\delta = 0$) show a linear dependence between P_L and R_e^{-1} that is valid for droplets as small as 0.86 nm in radius. To validate this apparent linearity, we insert the Tolman length correction into the Young-Laplace equation and find that δ is positive and small with a value of 0.055 ± 0.021 nm. Moreover, γ_p values for $T \geq 220$ K from this thermodynamic route, regardless of whether we assume δ is zero or not, are consistent with the extrapolation of γ_p obtained for TIP4P/2005 using the test-area method,[44] a thermodynamic method, as shown in Fig. 5(a).

We compute γ_p from the mechanical approach by first finding γ_s and R_s using Eqs. (8) and (9), then by using Eqs. (11) and (12), which produces consistent but noisier results, and finally by using Eqs. (13) and (12). For our range of T and N, we show that γ_s decreases as R_s decreases. Fitting these results with Eq. (2) results in positive and rather large values of $\delta = 0.32 \pm 0.02$ nm from Fig. 8(a) and $\delta = 0.21 \pm 0.01$ nm from Fig. 9(a). Although these two values do not overlap within error, they both suggest that δ from the mechanical route is significantly larger than the value from the
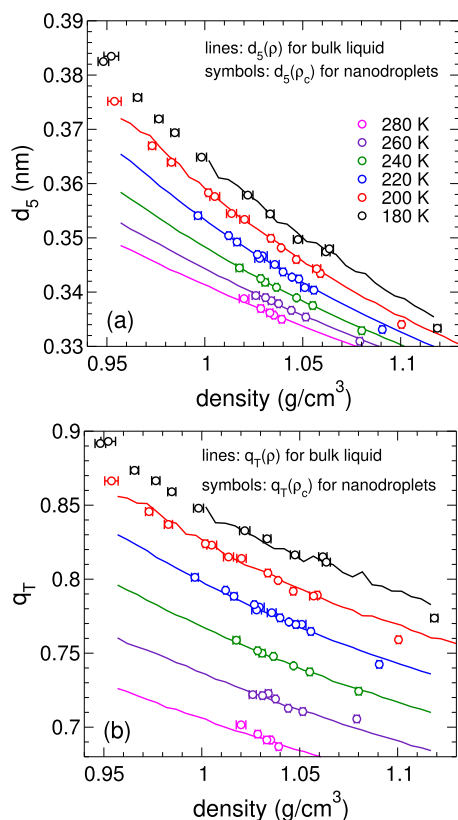

FIG. 11. Local measures of structure (a) d_5 and (b) q_T as functions of density. Symbols indicate data for nanodroplets, while curves show results for bulk. At $T = 180$ K, it is difficult to equilibrate the bulk liquid at low density.

thermodynamic route. Moreover, estimates of γ_p obtained from fitting mechanical-route results tend to be higher than thermodynamic-route results, as apparent in Fig. 5(b). However, if we consider γ_s from Eq. (13) as a function of R_s^{-1} as shown in Fig. 9(a), the γ_p values resulting from fitting with Eq. (2) are consistent with the thermodynamic route and with Vega and de Miguel's extrapolation for $T \geq 240$ K.

We also conclude that γ_s from the thermodynamic route remains relatively constant as we vary R_e for $T \geq 220$ K but shows larger variation at $T = 200$ and 180 K, where it changes by 15% over the range of droplet sizes we use. By contrast, γ_s from the mechanical route increases significantly with R_e, resulting in almost a 50% change in γ_s at $T = 180$ K. These results are equivalent to δ being small for the thermodynamic route and large for the mechanical route.

At 300 K, our thermodynamic results for γ_s as a function of droplet size are consistent with those of Lau *et al.*,[20] while those from the mechanical route are not. One might conclude, therefore, that the mechanical route for determining γ_s and δ lacks validity, and the relatively large value of $\delta = 0.2$–0.3 nm should be rejected in favor of the smaller value of $\delta \approx 0.06$ determined from the thermodynamic route. However, as δ is the difference between R_e and R_s, which is understood to be where the surface tension acts, values in the range of 0.2–0.3 nm are reasonable given the locations of R_e and the negative pressure minima in Fig. 1. In sum, our work confirms the discrepancy between the mechanical and thermodynamic routes that has been previously noted in the literature and so supports the need for a better theoretical understanding of the connection between the two.

The marked increase in γ_p for $T < 220$, as shown in Fig. 5, approximately coincides with the crossing of the Widom line at $T = 230$ K for bulk TIP4P/2005 water at ambient pressure[45] and hence is correlated with the LLPT occurring in this water model. This increase in γ_p is consistent across both the mechanical and thermodynamic routes. Our results thus confirm the scenario predicted theoretically in Refs. 25–27, in which γ_p increases more rapidly with decreasing T when the system enters the T regime below the Widom line where LDL-like properties begin to dominate the bulk behavior. We also note that Ref. 26 predicts that the surface of a deeply supercooled water nanodroplet will exhibit a dense surface layer relative to the bulklike density of the droplet interior. This prediction is confirmed by the density profiles presented in Ref. 37 and is consistent with the radial variation of the structural properties presented in Sec. VI. The sudden increase in γ_p at low T that we infer from our droplet simulations was also observed in simulations of planar interfaces using the WAIL potential for (Water potential from Adaptive force matching for Ice and Liquid) water and was also interpreted as evidence for the LLPT scenario.[54]

Characterizing how local structure varies with radial distance from the center of the droplet with d_5 and q_T, we see behavior consistent with the formation of a well-ordered random tetrahedral network at low T and large N within droplet interiors. Furthermore, the dependence of these structural measures on local density matches that of bulk TIP4P/2005 water. Hence, from a structural perspective, the interiors of our nanodroplets are characteristic of the bulk.

We conclude that γ_s and R_s determined from the mechanical route are smaller than the values evaluated in the thermodynamic route, leading to larger values of δ and γ_p. However, both routes give

a positive value of δ for our range of T and N and suggest that δ is independent of T. Moreover, assuming the validity of the thermodynamic route, for $R_e \geq 1$ nm, we can ignore the curvature correction and use the planar surface tension to estimate the Laplace pressure inside water nanodroplets to within 15% down to 180 K. This last point is of practical importance for the estimation of the interior pressure in real water nanodroplets, for which the Laplace pressure is not easily measured directly.

REFERENCES

[1] M. Baker, Science **276**, 1072–1078 (1997).

[2] Ø. Wilhelmsen, T. T. Trinh, A. Lervik, V. K. Badam, S. Kjelstrup, and D. Bedeaux, Phys. Rev. E **93**, 032801 (2016).

[3] H. Ohno, N. Nishimura, K. Yamada, Y. Shimizu, S. Iwase, J. Sugenoya, and M. Sato, Skin Res. Technol. **19**, 375 (2013).

[4] S. Tachibana, A. Kouchi, T. Hama, Y. Oba, L. Piani, I. Sugawara, Y. Endo, H. Hidaka, Y. Kimura, K. Murata, H. Yurimoto, and N. Watanabe, Sci. Adv. **3**, eaao2538 (2017).

[5] W. Klemperer and V. Vaida, Proc. Natl. Acad. Sci. U. S. A. **103**, 10584–10588 (2006).

[6] M. Kulmala, Science **302**, 1000 (2003).

[7] P. G. Debenedetti, *Metastable Liquids: Concepts and Principles* (Princeton University Press, Princeton, 1996).

[8] T. Young, Philos. Trans. R. Soc. London **95**, 65 (1805).

[9] P. S. M. de Laplace, *Traité De Mécanique Céleste* (Courcier, Paris, 1805), Vol. 4, Supplément a la Théorie de l'Action Capillaire.

[10] J. S. Rowlinson and B. Widom, *Molecular Theory of Capillarity* (Dover Publications, Inc., New York, 1982).

[11] R. C. Tolman, J. Chem. Phys. **17**, 333 (1949).

[12] A. E. van Giessen and E. M. Blokhuis, J. Chem. Phys. **131**, 164705 (2009).

[13] E. M. Blokhuis and A. E. van Giessen, J. Phys.: Condens. Matter **25**, 225003 (2013).

[14] Ø. Wilhelmsen, D. Bedeaux, and D. Reguera, J. Chem. Phys. **142**, 064706 (2015).

[15] H. Yan, J. Wei, S. Cui, S. Xu, Z. Sun, and R. Zhu, Russ. J. Phys. Chem. A **90**, 635 (2016).

[16] K. Leong and F. Wang, J. Phys. Chem. **148**, 144503 (2018).

[17] F. Wang, O. Akin-Ojo, E. Pinnick, and Y. Song, Mol. Simul. **37**, 591 (2011).

[18] M. N. Joswiak, N. Duff, M. F. Doherty, and B. Peters, J. Chem. Phys. Lett. **4**, 4267 (2013).

[19] V. Molinero and E. B. Moore, J. Phys. Chem. B **113**, 4008 (2009).

[20] G. V. Lau, I. J. Ford, P. A. Hunt, E. A. Müller, and G. Jackson, J. Chem. Phys. **142**, 114701 (2015).

[21] J. L. F. Abascal and C. Vega, J. Chem. Phys. **123**, 234505 (2005).

[22] G. Menzl, M. A. Gonzalez, P. Geigera, F. Caupin, J. L. F. Abascal, C. Valeriani, and C. Dellago, Proc. Natl. Acad. Sci. U. S. A. **113**, 13582 (2016).

[23] S. H. Min and M. L. Berkowitz, J. Phys. Chem. **150**, 054501 (2019).

[24] P. H. Poole, F. Sciortino, U. Essmann, and H. E. Stanley, Nature **360**, 324 (1992).

[25] M. R. Feeney and P. G. Debenedetti, Ind. Eng. Chem. Res. **42**, 6396 (2003).

[26] J. Hrubý, "Nucleation and a new thermodynamic model of supercooled water," in *Proceedings of the 16th International Conference on Nucleation and Atmospheric Aerosols, Kyoto, 26–30 July 2004*, edited by M. Kasahara and M. Kulmala (Kyoto University Press, 2004).

[27] J. Hrubý and V. Holten, "A two-structure model of thermodynamic properties and surface tension of supercooled water," in Proceedings of the 14th International Conference on the Properties of Water and Steam, 2005.

[28] Y. Lü and B. Wei, Sci. China: Phys., Mech. Astron. **49**, 616 (2006).

[29] Y. J. Lü and B. Wei, Appl. Phys. Lett. **89**, 164106 (2006).

[30] F. Chen and P. E. Smith, J. Chem. Phys. **126**, 221101 (2007).

[31] L. Viererblová and J. Kolafa, Phys. Chem. Chem. Phys. **13**, 19925 (2011).

[32] J. Hrubý, V. Vinš, R. Mareš, J. Hykl, and J. Kalov, J. Phys. Chem. Lett. **5**, 425 (2014).

[33] V. Vinš, M. Fransen, J. Hykl, and J. Hrubý, J. Phys. Chem. B **119**, 5567 (2015).

[34] V. Vinš, J. Hošek, J. Hykl, and J. Hrubý, J. Chem. Eng. Data **62**, 3823 (2017).

[35] K. H. Kim, A. Späh, H. Pathak, F. Perakis, D. Mariedahl, K. Amann-Winkel, J. A. Sellberg, J. H. Lee, S. Kim, J. Park, K. H. Nam, T. Katayama, and A. Nilsson, Science **358**, 1589 (2017).

[36] S. M. Thompson, K. E. Gubbins, J. P. R. B. Walton, R. A. R. Chantry, and J. S. Rowlinson, J. Phys. Chem. **81**, 530 (1984).

[37] S. M. A. Malek, P. H. Poole, and I. Saika-Voivod, Nat. Commun. **9**, 2402 (2018).

[38] H. J. C. Berendsen, D. van der Spoel, and R. van Druren, Comput. Phys. Commun. **91**, 43 (1995); E. Lindahl, B. Hess, and D. van der Spoel, J. Mol. Model. **7**, 306 (2001); D. van der Spoel, E. Lindahl, B. Hess, G. Groenhof, A. E. Mark, and H. J. C. Berendsen, J. Comput. Chem. **26**, 1701 (2005); B. Hess, C. Kutzner, D. van der Spoel, and E. Lindahl, J. Chem. Theory Comput. **4**, 435 (2008).

[39] S. M. A. Malek, R. K. Bowles, I. Saika-Voivod, F. Sciortino, and P. H. Poole, Eur. Phys. J. E **40**, 98 (2017).

[40] I. Saika-Voivod, F. Smallenburg, and F. Sciortino, J. Chem. Phys. **139**, 234901 (2013).

[41] S. M. A. Malek, F. Sciortino, P. H. Poole, and I. Saika-Voivod, J. Phys.: Condens. Matter **30**, 144005 (2018).

[42] T. Nakamura, W. Shinoda, and T. Ikeshoji, J. Chem. Phys. **135**, 094106 (2011).

[43] J. Irving and J. Kirkwood, J. Chem. Phys. **18**, 817 (1950).

[44] C. Vega and E. de Miguel, J. Chem. Phys. **126**, 154707 (2007).

[45] J. L. F. Abascal and C. Vega, J. Chem. Phys. **133**, 234502 (2010).

[46] V. M. Samsonov, A. N. Bazulev, and N. Y. Sdobnyakov, Dokl. Phys. Chem. **389**, 83 (2003).

[47] A. Ghoufi and P. Malfreyt, J. Chem. Phys. **135**, 104105 (2011).

[48] G. V. Lau, P. A. Hunt, E. A. Müller, G. Jackson, and I. J. Ford, J. Chem. Phys. **143**, 244709 (2015).

[49] J. G. Sampayo, A. Malijevsky, E. A. Müller, E. de Miguel, and G. Jackson, J. Chem. Phys. **132**, 141101 (2010).

[50] A. Malijevsky and G. Jackson, J. Phys: Condens. Matter **24**, 464121 (2012).

[51] I. Saika-Voivod, F. Sciortino, and P. H. Poole, Phys. Rev. E **63**, 011202 (2001).

[52] P. L. Chau and A. J. Hardwick, Mol. Phys. **93**, 511 (1998).

[53] C. H. Rycroft, Chaos **19**, 041111 (2009).

[54] T. R. Rogers, K.-Y. Leong, and F. Wang, Sci. Rep. **6**, 33284 (2016).